MethodsX 11 (2023) 102305

Contents lists available at ScienceDirect

MethodsX

journal homepage: www.elsevier.com/locate/methodsx

Deriving new mixing ratios for Venus atmospheric gases using data from the Pioneer Venus Large Probe Neutral Mass Spectrometer ☆

R. Mogul [a,b,*], G. Avice [c], S.S. Limaye [d], M.J. Way [e,f,g]

[a] Chemistry & Biochemistry Department, California State Polytechnic University, Pomona, CA, USA
[b] Blue Marble Institute of Science, Seattle, WA USA
[c] Université Paris Cité, Institut de physique du globe de Paris, CNRS, Paris, F-75005, France
[d] Space Science and Engineering Center, University of Wisconsin, Madison, WI, USA
[e] NASA Goddard Institute for Space Studies, 2880 Broadway, New York, NY, USA
[f] GSFC Sellers Exoplanet Environments Collaboration, Greenbelt, MD, USA
[g] Theoretical Astrophysics, Department of Physics and Astronomy, Uppsala University, Uppsala, Sweden

ARTICLE INFO

Method name:
Deriving Mixing Ratios, Volume Percent Values, and Densities

Keywords:
Venus
Atmosphere
Mixing ratios
Density
Mass spectrometry

ABSTRACT

We present the first published method to convert data obtained by the Pioneer Venus Large Probe Neutral Mass Spectrometer (LNMS) into units of mixing ratio (ppm) and volume percent (v%) against CO_2 and N_2, the dominant Venus atmospheric gases, including conversion to density (kg m^{-3}). These unit conversions are key to unlocking the untapped potential of the data, which represents a significant challenge given the scant calibration data in the literature. Herein, we show that our data treatments and conversions yield mixing ratios and volume percent values for H_2O, N_2, and SO_2 that are within error to those reported for the gas chromatograph (LGC) on the Pioneer Venus Large Probe (PVLP). For the noble gases, we developed strategies to correct for instrument biases by treating the data as a relative scale and using PVLP and Venera-based measurements as calibration points. Together, these methods, conversions, calibrations, and comparisons afford novel unit conversions for the LNMS data and yield unified measures for Venus' atmosphere from the LNMS and LGC on the PVLP.

- Conversion into mixing ratio (ppm), volume percent (v%), and density (kg m^{-3}).
- Mixing ratios are expressed against CO_2 and N_2.
- LNMS and LGC measurements on the PVLP are consistent.

☆ **Related Research Article** Mogul, R., Limaye, S.S. & Way, M.J. The CO_2 profile and analytical model for the Pioneer Venus Large Probe neutral mass spectrometer. Icarus, **392** (2023), pp. 115374. https://doi.org/10.1016/j.icarus.2022.115374
DOI of original article: 10.1016/j.icarus.2022.115374

* Corresponding author.
E-mail address: rmogul@cpp.edu (R. Mogul).
Social media: (R. Mogul)

https://doi.org/10.1016/j.mex.2023.102305
Received 29 June 2023; Accepted 28 July 2023
Available online 28 July 2023

Specifications table

Subject area:	Earth and Planetary Sciences
More specific subject area:	*Atmosphere of Venus*
Name of your method:	*Deriving Mixing Ratios, Volume Percent Values, and Densities*
Name and reference of original method:	*Mogul, R., Limaye, S.S. & Way, M.J. The CO_2 profile and analytical model for the Pioneer Venus Large Probe Neutral Mass Spectrometer. Icarus, 392 (2023), pp. 115374* https://doi.org/10.1016/j.icarus.2022.115374
Resource availability:	https://nssdc.gsfc.nasa.gov/nmc/dataset/display.action?id=PSPA-00649

Method details

Rationale

We present a new methodological procedure to convert data obtained by the Pioneer Venus Large Probe Neutral Mass Spectrometer (LNMS) into units of atmospheric mixing ratio (ppm) and volume percent (v%) against CO_2 and N_2, the dominant Venus atmospheric gases, including conversion to density (kg m^{-3}). These units were not published in the original LNMS investigations, which spanned 1979–1993 and described the instrument [1,2], initial results [3–5], and ensuing data analyses [6–9]. Hence, our study represents a significant advance towards unlocking the untapped potential of the LNMS mass spectral data. For example, in Mogul *et al.* 2021 [10], we extracted novel chemical trends from the LNMS data that are suggestive of redox disequilibria within the cloud deck. In Mogul *et al.* 2023 [11], we extracted the most detailed altitude profile for CO_2, to date, and supported the potential presence of a near-surface particle haze layer. In this report, we detail means to enact the unit conversions to mixing ratio (ppm), volume percent (v%), and density (kg m^{-3}), which represent significant challenges given the absence of detailed calibration data regarding ionization, ion transmission, and ion conductance rates in the LNMS.

Background

The Large Probe Neutral Mass Spectrometer (LNMS) was a magnetic sector and electron ionization mass spectrometer onboard the NASA Pioneer Venus Large Probe (PVLP), which descended through Venus' atmosphere in 1978 [1,2,5]. Upon entry into Venus' atmosphere, the LNMS obtained a total of 56 spectra, which included 4 background spectra obtained just prior to atmospheric sampling (pre-sampling spectra; ~200–64 km), and 52 spectra obtained during atmospheric sampling between the altitudes of 64.2–0.2 km (descent profile). The LNMS operations also included a pre-programmed Isotope Ratio Measuring (IRM) sequence for noble gases, which involved the collection of atmospheric samples at ~62 km, scrubbing of the active gases, and analysis of the partly purified noble gases between ~48–45 km [1,5]. During sampling, electron ionizations were conducted at 70 eV (46 spectra) with additional pre-programmed ionizations at 30 eV (3 spectra) and 22 eV (3 spectra) during descent through the clouds (~54–53 km) and lower atmosphere (~30–28 and 9–8 km). Pre-sampling spectra were obtained at 70 eV. Positive ions produced from the respective electron ionizations were detected through use of separate low mass (*m/z* 1–16) and high mass (*m/z* 16–208) electron multiplier-counter channels[1], which afforded high sensitivity across a broad detectable mass range of *m/z* (1–208 u).

Ion count (counts) in the LNMS were measured at 232 *pre-selected* mass positions, which correlated to the masses of target species chosen during design and assembly of the LNMS. The pre-selected mass positions, which afforded rapid spectral acquisition during the descent, were *non-uniformly distributed* across *m/z* 1–208. Hence, by design, several mass positions – when considering a mass resolving power of 453 (9.4% separation) – were *not* measured by the LNMS across *m/z* 1–208. Rapid data collection (64 s) was controlled by the LNMS microprocessor, which involved a peak-stepping routine (59 s) across the *pre-selected* mass positions followed by a re-calibration step of the ion acceleration voltage (5 s). As suggested in prior reports [2,12], the respective ion profiles were collected over 235 ms and transmitted in units of counts to Earth by the PVLP.

Consistent with statements in Donahue et al., 1992 [7] and Hoffman et al., 1980 [5], and per our understanding after review of the laboratory notebooks of J.H. Hoffman at the University of Texas, Dallas, mixing ratios for target species (*e.g.*, Ne, H_2O, and H_2S) were then obtained by (1) calculation of the mixing ratio for ^{36}Ar ($\leq$24 km) using calibration data for CO_2 (the major Venus atmospheric gas) and ^{36}Ar (a trace Venus atmospheric gas), which were obtained on Earth using the LNMS flight spare, followed by (2) ratio-based comparisons of target species to the counts and calculated mixing ratio for ^{36}Ar. Therefore, the resultant mixing ratios in the original LNMS investigations [4,5,7] assumed similar behaviors of the target species to ^{36}Ar in the mass analyzer [7] and were not expressed against CO_2 and N_2 (a minor Venus atmospheric gas), despite the published equation in Hoffman et al., 1980 [5] that yields such an expression. This is significant since mixing ratios for Venus science are typically expressed against CO_2 and N_2, the dominant Venus atmospheric gases [13,14], which do not behave like ^{36}Ar in a mass analyzer (*e.g.* chemical getter activity [15]). Hence, in this study, we present the first published treatment for the LNMS data to yield atmospheric mixing ratios for target species against CO_2 and N_2.

[1] Per review by M. J. Way of the Pioneer Venus Large Probe Neutral Mass Spectrometer Final Report (April 1979) and Pioneer Venus Program Large & Small Probe Data Book (June 1976) in the Pioneer Venus archive at the NASA Ames Research Center.

Counts in the LNMS

Measured counts in the LNMS are related to density of a target species (i) in the analyzed sample (*e.g.*, kg m^{-3} or g mL^{-1}) through Eq. (1), which was adapted from the mathematical descriptions of the LNMS in Donahue et al., 1992 [7]. Through Eq. (1), counts in the LNMS for the target species at the altitude (a) of measurement (I_i^a) relate to the instrumental constant of the mass analyzer (A), transmission coefficient of the parent ion (v_i), ionization cross section of the target gas (σ_i), parent ion fraction (f_i) [or relative abundance of the parent ion among the total ionized target species (*e.g.*, multiple ionized and/or chemical fragment ions)], and ratio of the rates of mass flow intake (ψ_i^a; example units, g s^{-1}) and ion conductance (C_i^a; example units, mL s^{-1}) of the target ion into the mass analyzer at the altitude of measurement.

$$I_i^a = \left(A v_i \sigma_i f_i\right)\psi_i^a / C_i^a \tag{1}$$

Mass flow intake (ψ_i^a) and ion conductance (C_i^a) rates are treated as altitude-dependent and influenced by factors including the rapid atmospheric pressure changes (~0.1 to 90 bar in ~50 min) across the descent (64.4–0.2 km), related increases in mass flow intake into the ion source, and the pre-programmed closure of an intake valve at ~47 km (Valve 1 in the block diagram in Fig. 2 in Hoffman et al., 1979 [1]). Closure of Valve 1 significantly reduced mass flow intake into the ion source at the higher atmospheric pressures, which assisted in maintaining low pressures in the ion source and number density in the mass analyzer.

As adapted from Hoffman et al., 1980 [5], ion conductance rates are further defined as the fraction of ions ($C_i \approx C_{i_0} * (C_A/(C_A + C_V))_i$), which form after electron ionization (C_{i_0}) and that reach the detector and yield a measurable signal. Competing ion pathways in the LNMS include (1) passage of the ion through the ion optics slits into the mass analyzer to the detector (C_A), thereby yielding measurable counts, and (2) passage of the ion towards a chemical getter through a variable conductance valve (C_V), which was proximal to the ion source. The variable conductance valve opened to the chemical getter (zirconium-aluminum alloy) commensurately with increasing atmospheric pressure. Chemical getters are solid materials that retain ions through adsorption, absorption, and/or chemical reactions; getter active species include water, N_2, CO_2, and SO_2, while getter-inactive (or low activity) species include noble gases and hydrocarbons [15,16]. Opening of the variable conductance valve reduced the total number density entering the mass analyzer, which preserved detector sensitivity at the higher atmospheric pressures.

Normalization and background correction

Data are normalized at each altitude of measurement to either $^{136}Xe^{2+}$ (m/z 68) or $^{136}Xe^{+}$ (m/z 136) to account for the mass-dependent and altitude-dependent changes in transmission, as described in Mogul et al., 2023 [11]. The $^{136}Xe^{2+}$ and $^{136}Xe^{+}$ ions arise from the ionized internal calibrant gas (a pre-made mixture of ^{136}Xe and CH_4) used during calibration of the ion acceleration voltage after each mass sweep. We note that trends for $^{136}Xe^{3+}$ (m/z 45) indicate the presence of competing isobaric species [11]. Thus, for species with ≤ m/z 90 (*e.g.*, Kr, SO_2, CO_2, N_2, and H_2O), data are normalized to $^{136}Xe^{2+}$ (m/z 68). For species with > m/z 90 (*e.g.*, ^{131}Xe and ^{132}Xe), data are normalized to $^{136}Xe^{+}$ (m/z 136).

Data are corrected for background contributions by accounting for terrestrial contamination, residual noble gases arising from the IRM sequence (≤ 45.2 km), purging of noble gas contamination, closure of the intake valve (~47 km), and a temporary clog of the LNMS inlet/s (~50–25 km) [11]. For data collected between 64.4–25.9 km, background corrections are conducted using the respective pre-sampling value *or* the lowest successive value between 64.4–48.4 km, which accounts for purging of the terrestrial contaminants just prior to the IRM sequence measurement at 45.2 km. For example, for the noble gases, corrections using the pre-sampling averages yield negative values at several mass positions at multiple altitudes, which is indicative of overcorrection. Such trends suggest that the background noble gases purge after the successive mass sweeps during sampling. This assessment is consistent with trends extracted from the four successive pre-sampling spectra [11], which show decreases of ~37 and 41% in the counts for ^{40}Ar and ^{86}Kr, respectively. Analogously, for data collected between 24.4–0.2 km – *after* the closure of Valve 1, conclusion of the IRM sequence, and dispersing of the clogged inlet/s (or resumption of nominal intake) – background corrections are conducted using the lowest successive value measured between 39.3–0.2 km. For the data at ≤ 24.4 km, this treatment prevents overcorrection (and the acquisition of negative values) by accounting for the noble gases arising from the IRM sequence, which temporarily increase in counts at 45.2 km and subsequently decrease, or purge, at differing rates across the following measurements in the descent profile.

Conversion to mixing ratio

In Eq. (2), mixing ratios are obtained by expressing the number density of the target gas (n_i) against the summed number densities of CO_2 (n_{CO_2}) and N_2 (n_{N_2}), and multiplying by 1×10^6 to yield units of ppm. In Eq. (3), the number density for the target gas (n_i) is the product between the target-specific sensitivity factor (p_i) and counts for the respective parent ion from the LNMS (I_i), as adapted from prior mathematical descriptions in Hoffman et al., 1980 [5] and Donahue et al., 1992 [7]. The sensitivity factor (p_i) accounts for differences in ionization, mass flow, and conductance between the target gas and chosen gas standard – which is CO_2 in this study, consistent with the use of CO_2 in Hoffman et al., 1980 [5], but contrary to the choice of ^{36}Ar in Donahue et al., 1992 [7].

$$(mixing\ ratio)_i = \frac{n_i}{n_{CO_2} + n_{N_2}} \tag{2}$$

$$n_i = p_i I_i \tag{3}$$

We estimate the sensitivity factor for differing targets in the LNMS using the relationship described in Eq. (4), which is adapted from Hoffman et al., 1980 [5] and Donahue et al., 1992 [7] and equates the ratio of the number densities for the target species and CO_2 (n_i /n_{CO_2}) to the ratio of mass flow intake rates (ψ_i /ψ_{CO_2}), and the product of p_i and the reciprocal of the ratio of the measured counts (I_{CO_2} /I_i). We obtain an expanded expression for ρ_i^a at the altitude of measurement by:

(1) Rearrangement of the equalities in Eq. (4) to yield Eq. (5) (consistent with the strategy in Donahue et al., 1992 [7]);
(2) Substitution of Eq. (1) for the I_{CO_2} and I_i terms to obtain Eq. (6); and
(3) Ensuing reduction to yield Eq. (7).

To account for potential uncertainties in ρ_i^a, we introduce several correction factors in Eq. (8) inclusive of α_i for the ratio of transmission coefficients, β_i for the ratio of the parent ion fractions, and γ_i^a for the ratio of the ion conductance rates.

$$\frac{n_i}{n_{CO_2}} = \frac{\psi_i}{\psi_{CO_2}} = \rho\left(\frac{I_i}{I_{CO_2}}\right) \tag{4}$$

$$\rho = \left(\frac{\psi_i}{\psi_{CO_2}}\right)\left(\frac{I_{CO_2}}{I_i}\right) \tag{5}$$

$$\rho_i^a = \left(\frac{\psi_i}{\psi_{CO_2}}\right)^a \left(\frac{A}{A}\right)\left(\frac{\upsilon_{CO_2}}{\upsilon_i}\right)\left(\frac{\sigma_{CO_2}}{\sigma_i}\right)\left(\frac{f_{CO_2}}{f_i}\right)\left(\frac{\psi_{CO_2}}{\psi_i}\right)^a \left(\frac{C_i}{C_{CO_2}}\right)^a \tag{6}$$

$$\rho_i^a = \left(\frac{\upsilon_{CO_2}}{\upsilon_i}\right)\left(\frac{\sigma_{CO_2}}{\sigma_i}\right)\left(\frac{f_{CO_2}}{f_i}\right)\left(\frac{C_i}{C_{CO_2}}\right)^a \tag{7}$$

$$\rho_i^a = \alpha_i\left(\frac{\upsilon_{CO_2}}{\upsilon_i}\right)\left(\frac{\sigma_{CO_2}}{\sigma_i}\right)\beta_i\left(\frac{f_{CO_2}}{f_i}\right)\gamma_i^a\left(\frac{C_i}{C_{CO_2}}\right) \tag{8}$$

In the following bullet list, we detail steps for obtaining estimates of ρ_i^a. These steps include the acquisition of key parameters by interpolation, reliance on assumptions from the original LNMS investigations, and extraction of trends from the pre-sampling spectra.

- The *transmission coefficient* for the target species (υ_i) is obtained by interpolation using published LNMS reference data for non-polar gases [7]. For target species with *m/z* 15–50 (*e.g.*, H_2O, HDO, N_2, H_2S, and CO_2), we obtain the transmission coefficient by interpolation through linear regression of the reference data across *m/z* 15–40 ($R^2 = 0.9966$), as shown in Fig. 1A. The associated uncertainty of the measure is obtained using the standard error of the regression (±0.1). For target species with higher masses (~ *m/z* 50–131; *e.g.*, SO_2, Kr, and Xe) – *which fall outside the linear trend observed in Fig. 1A between m/z 15–40* – we obtain the transmission coefficient through interpolation and non-linear regression across *m/z* 2–131 ($R^2 = 0.9975$), as described and shown in Fig. 1B. Given the lack of data points between *m/z* 50 and 131 in the reference transmission data, we assume a standard 1 σ error (± 34.1%) for species with *m/z* 50- 130. To account for uncertainties in these total assumptions, we include α_i (Eq. (8).) as a correction factor to adjust for differences in getter activity of the target species, detector biases, and other influences.
- The *parent ion fraction* (f_i) is obtained from the pre-sampling data, descent profile, or NIST database (70 eV). In the LNMS, ionization yields for double ionization of noble gases are higher than those reported in the NIST database [11]. Hence, f_i for He, Ar and Xe are obtained using the pre-sampling data, which contain sufficient counts for ^{4}He (a terrestrial contaminant), ^{40}Ar, ^{38}Ar, and ^{36}Ar (terrestrial contaminants), and ^{136}Xe (internal calibrant). For Ne (*m/z* 20) and Kr (*m/z* 68), f_i are estimated by interpolation using the LNMS trends across He, Ar, and Xe; no counts were measured for Ne^{2+} in the pre-sampling data, potentially due to collisional loss, and *m/z* 43 (for $^{86}Kr^{2+}$) was not a measured mass position. For polyatomic ions, fragmentation patterns for CH_4 (all fragments), H_2O (OH^+/H_2O^+ ratio), and CO_2 ($CO^+/CO_2{}^+$ ratio at ≤24 km) in the LNMS are within error to trends from the NIST database [11]. Hence, values of f_i for target polyatomic gases with incomplete representation of the respective fragments (due to the choice of pre-selected mass positions) are extracted from the NIST database. To account for uncertainties in these assumptions we include β_i (Eq. (8).) as a correction factor and assume 5% error to account for descent-related fluctuations.
- *Cross sections* (σ) at 70 eV for polyatomic gases are obtained from the NIST database [17]. Cross sections for the noble gases are obtained from Rapp *et al.*, 1965 [18]. Cross sections are treated as standards with minimal to negligible error.
- *Ion conductance rates* are simplified using the relationship of $C_i \approx m_i^{-1/2}$ for non-gettered species (*e.g., e.g.*, noble gases and methane) from Donahue et al., 1992 [7], which is then applied to getter-active species (*e.g.*, active chemicals such as CO_2, N_2, H_2O, and H_2 [15]) and corrected for necessary changes using γ_i^a ($C_i \approx \gamma_i^a(m_i^{-1/2})$).
- The *bulk correction factor* at the altitude of measurement (k_i^a) in Eq. (9) is then obtained by combining the discreet correction factors of α_i, β_i, and γ_i^a, followed by substitution into Eq. (8) to yield Eq. (10).

$$k_i^a = \alpha_i\beta_i\gamma_i^a \tag{9}$$

$$\rho_i^a = k_i^a\left(\frac{\upsilon_{CO_2}}{\upsilon_i}\right)\left(\frac{f_{CO_2}}{f_i}\right)\left(\frac{\sigma_{CO_2}}{\sigma_i}\right)\left(\frac{m_{CO_2}}{m_i}\right)^{1/2} \tag{10}$$

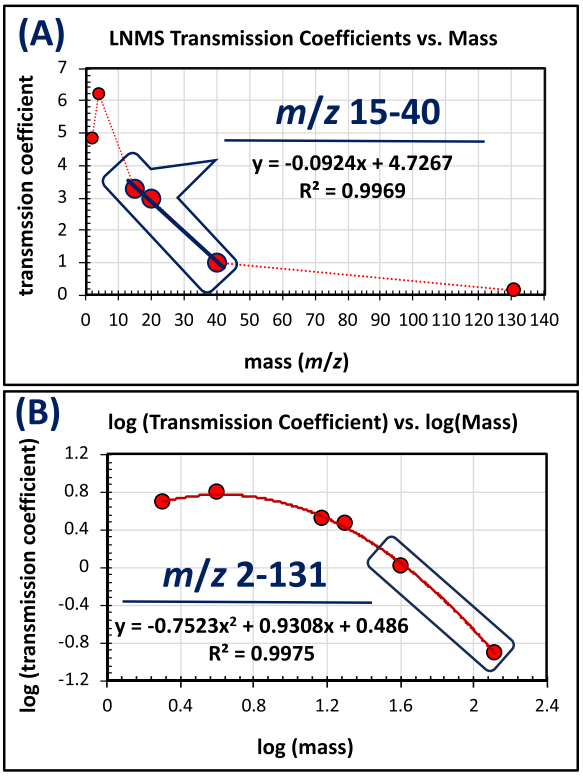

Fig. 1. The LNMS transmission coefficients (red circles) for H_2^+, $^4He^+$, CH_3^+, $^{20}Ne^+$, $^{40}Ar^+$, and $^{131}Xe^+$ (red circles) from Fig. 5 in Donahue et al., 1992 are plotted against mass in panel (A) to show the linear trend (blue callout box, thick blue line, $R^2 = 0.9966$) between *m/z* 15–40 (larger red circles), which is used to obtain transmission coefficients for target species of *m/z* 15–40, and in panel (B) as a log-log plot to show the 2nd order polynomial relationship across *m/z* 2–131 ($R^2 = 0.9975$), which is used to obtain transmission coefficients for targets with *m/z* ~50–136 (blue box).

Mixing ratios at the altitude of measurement are thus obtained using Eq. (11), which affords a relative scale for the LNMS data by combining Eqs. (2), (3), and (10) and assuming a relationship of $n_{CO_2} = I_{CO_2}$. At current, propagation of errors, inclusive of I_i [11], yields mixing ratios with uncertainties of:

(1) ~17% for targets with *m/z* 15–50 represented by ≥ 3 mass positions in the data and fit to Gaussian functions [11];
(2) ~22% for targets with *m/z* 15–50 represented by ≤ 2 mass positions; and
(3) ~38% for targets with > *m/z* 50.

In the following sections, we detail methods to estimate the bulk correction factor (k_i^a) for differing target gases.

$$\left((mixing\ ratio)_i\right)^a = \left(\frac{p_i I_i}{n_{CO_2} + n_{N_2}}\right)^a = k_i^a \left(\frac{(I_i)\left(\frac{v_{CO_2}}{v_i}\right)\left(\frac{\sigma_{CO_2}}{\sigma_i}\right)\left(\frac{f_{CO_2}}{f_i}\right)\left(\frac{m_{CO_2}}{m_i}\right)^{1/2}}{I^a_{CO_2} + n^a_{N_2}}\right) \tag{11}$$

$$\left((mixing\ ratio)^{atmos}\right)^a = k_i^a \left((mixing\ ratio)^{calc}\right)^a \tag{12}$$

Corrections for active gases

To ascertain the necessity to correct the mixing ratios for active gases (*e.g.,* H_2O, N_2, and SO_2), or obtain values for k_i^a, we use Eq. (12) and compare our calculated mixing ratios ($(mixing\ ratio)^{calc}$) to accepted atmospheric values from the literature ($(mixing\ ratio)^{atmos}$). Our comparisons for the active gases suggest that $k_i^a \approx 1$ at differing masses and at differing altitudes. In Table 1, we compare our mixing ratios or volume percent for H_2O, N_2, and SO_2 to measures from differing spacecraft and altitudes. For H_2O, our respective mixing ratios are within error to measures from the LGC at 51.6 km and 21.6 km [19,20]. For N_2, our respective volume percent values are within error to measures from the LGC at 51.6 km [19,20] and the V11/12 at 23.0 km [21]. For SO_2, our respective mixing ratios are within error to measures from the PV Orbiter UV Spectrometer (PV OUVS) at 58 km [22] and LGC at 21.6 km [19,20]. For the active gases, these comparisons suggest that corrections are *unnecessary* for the ratio of transmission coefficients (α_i), parent ion fraction (β_i), and ratio of ion conductance rates (γ_i^a), inclusive of adjustments for altitude.

Table 1
Comparison of mixing ratios or volume percent for H_2O, N_2, and SO_2 from this study and the PV LGC, V11/12 EI-MS, and PV OUVS at differing altitudes (*a*), where uncertainties represent the propagated (this study) or published errors.

Target Gas	Mixing Ratio or Volume Percent		
(mass)	LNMS	Comparison	Comments
H_2O (*m/z* 18)	**ppm**	**ppm**	**other *in situ* measures**
H_2O (*a* = 51.3 km)	243 ± 42	<600	PVLP, LGC, 51.6 km [19,20]
H_2O (*a* = 21.6 km)	1560 ± 269	1350 ± 150	PVLP, LGC, 21.6 km [19,20]
N_2 (*m/z* 28)	**v%**	**v%**	
N_2 (*a* = 51.3 km)	3.87 ± 0.68	4.60 ± 0.14	PVLP, LGC, 51.6 km [19,20]
N_2 (*a* = 24.4 km)	3.47 ± 0.61	4.50 ± 0.50	V11/12, EIMS, 23 km [21]
SO_2 (*m/z* 64)	**ppm**	**ppm**	
SO_2 (*a* = 51.3 km)	3 ± 1	4	PV, OUVS, 58 km [22]
SO_2 (*a* = 21.6 km)	396 ± 160	185^{+350}_{-155}	PVLP, LGC, 21.6 km [19,20]

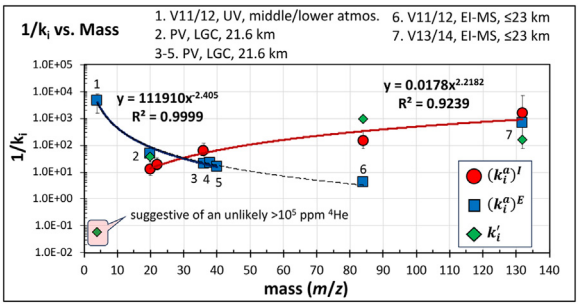

Fig. 2. Plots of the reciprocal of the bulk correction factors $(k_i^a)^I$ (internal scale, I), $(k_i^a)^E$ (external scale, E), and k_i' (original LNMS conversion factors) against mass of ^{4}He, ^{20}Ne, ^{36,38,40}Ar, and ^{132}Xe. Values for $(k_i^a)^I$ (red circles) are obtained by comparison to prior LNMS values and fit by power regression (red line; $R^2 = 0.9239$). Values for $(k_i^a)^E$ (blue squares) are obtained by comparison to other *in situ* spacecraft measures (listed and identified as 1–6) and fit by power regression across *m/z* 4–40 (1–5; blue line; $R^2 = 0.9999$) and *m/z* 4–84 (1–6; dashed blue line; $R^2 = 0.9998$). Values for k_i' (green diamonds) are inferred from Hoffman et al., 1980 and Donahue et al., 1981. Error bars represent the propagated errors.

Corrections for noble gases and methane

The noble gases and methane exhibit limited degrees of getter retention [8,15]. Hence, we ascertain the need for corrections using Eq. (12) by comparing our calculated mixing ratios to those from (A) the original LNMS investigations (*i.e.*, an internal scale) and (B) other *in situ* spacecraft-based measures (*i.e.*, an external scale). Estimations of k_i^a for the noble gases across the internal and external scales yield a range of $\sim 10^{-2}$–10^{-4} (Fig. 2), which indicates a need for substantial corrections – consistent with observations described in Donahue *et al.*, 1981 [6] and Donahue et al., 1992 [7]. The corrections likely correlate to adjustments to the ratio of ion conductance rates (γ_i^a) and to a lesser degree to the ratio of transmission coefficients (α_i) given the difference in ion transmission pathways induced by the getter and ion pumping activities of CO_2^+ when compared to the noble gases and methyl ions [8].

Using the internal scale (*I*), we obtain $(k_i^a)^I$ by comparing species with ≥ *m/z* 15 (such as ^{20}Ne, ^{22}Ne, ^{36}Ar, ^{84}Kr, and ^{132}Xe), which were detected in the high mass channel, to values from the original LNMS investigations in Hoffman et al., 1980 [5], Donahue et al., 1981 [6], and Donahue et al., 1992 [7]. We additionally extract the original conversion factors used in Hoffman et al., 1980 [5] and Donahue et al., 1981 [6] for the noble gases, which we define as k_i'. The original conversion factors, per our understanding ($k_i' = X_i/^{36}Ar$), were defined as the ratio of averaged counts between the major noble gas isotope (X_i = ^{20}Ne, ^{84}Kr, and ^{132}Xe) and ^{36}Ar at ≤24 km and/or <5 km.

In Fig. 2, we display plots against mass for the reciprocal of $(k_i^a)^I$ and reciprocal of the averaged k_i' from ≤ 2 km (which exhibits less scatter when compared to ≤ 5 km). Similar non-linear trends are observed between $(k_i^a)^I$ (red circles) and k_i' (green diamonds), which supports the relationship of $(k_i^a)^I \approx k_i'$. Such trends validate our treatment of the noble gases in the LNMS. Power regression trends for $1/(k_i^a)^I$ against mass ($R^2 = 0.9239$; Fig. 2) suggest a mass-dependent behavior for the noble gases throughout ion pumping and/or detection – which is congruent with relationship of $C_i \approx m_i^{-1/2}$. For detection of noble gases in the high mass channel, these trends suggest that higher masses correlate to higher outputted counts and require greater correction.

When extending the trends to He, which was measured by the low mass channel, we obtain untenable mixing ratios of $\sim 10^5$–10^6 ppm, as obtained by extrapolation for $(k_i^a)^I$ or direct calculation for k_i'. These trends suggest that the LNMS conversion factors fail for He (k_i'), or that the LNMS is contaminated with terrestrial He at relative abundances that far exceed background counts from the pre-sampling spectra. This is relevant since the LGC vented He carrier gas during operation (~60 min) into the PVLP interior [11,23]. In theory, He from the LGC discharge could have entered the LNMS [5,11]. During pre-launch storage (~5 months), He from the PVLP interior leaked into the LNMS at an approximate rate of $\sim 10^{12}$ cm^3 s^{-1} [5]. Such leak rates likely preclude significant He

contamination from the LGC discharge over the ~1 hr operation time. In addition, background corrections using the pre-sampling spectra yield negative values for He at 49.4 and 48.4 km. Further, decreases of ~3-fold in He counts are observed *after* the IRM sequence across 45.2 to 25.9 km. These combined trends suggest that purging rates for He are greater than any potential diffusion rates of He into the LNMS.

Therefore, to better understand the behavior of He in the LNMS, we used an external scale (*E*) to obtain $(k_i^a)^E$ for the noble gases across *m/z* 4–40. We detail acquisition of $(k_i^a)^E$ for ^{4}He, ^{20}Ne, ^{22}Ne, ^{36}Ar, ^{38}Ar, ^{40}Ar, ^{86}Kr, and Xe (^{131}Xe + ^{132}Xe) in the following bullet list.

- We obtain $(k_i^a)^E$ for ^{4}He ($a \leq 24.4$ km) by comparing calculated mixing ratios for ^{4}He at ≤24 km to published values for He from the middle and lower atmosphere (9 ± 6 ppm; ~60 km to the surface) from Krasnopolsky et al., 2005 [24], which were extracted from data acquired via UV spectroscopy by Venera 11 and 12 (V11/12). For LNMS, contributions from ^{3}He are considered insignificant given the calculated ^{3}He/^{4}He ratio of ~3.9 10^{-4} from the IRM samples.
- We obtain $(k_i^a)^E$ for ^{20}Ne ($a = 21.6$ km) by comparing the calculated mixing ratio for ^{20}Ne at 21.6 km to measures from the LGC for Ne at 21.6 km (4.31 ± 0.65 ppm) reported in Oyama *et al.*, 1980 [19]. The LGC mixing ratio was converted to ^{20}Ne using isotope abundances for Ne extracted in this study from the IRM data (92.70 ± 0.18% ^{20}Ne, 0.26 ± 0.03% ^{21}Ne, and 7.04 ± 0.15% ^{22}Ne), which was corrected for CO_2^{2+} at *m/z* 22 using respective counts for CO_2^+ and the averaged CO_2^{2+}/CO_2^+ ratio from the descent profile [11].
- We obtain respective $(k_i^a)^E$ values for ^{36}Ar, ^{38}Ar, and ^{40}Ar ($a = 21.6$ km) by comparing the calculated mixing ratios for ^{36}Ar, ^{38}Ar, and ^{40}Ar at 21.6 km to measures from the LGC for Ar at 21.6 km (67.2 ± 2.3 ppm) reported in Oyama *et al.*, 1980 [19]. The LGC mixing ratio for Ar was portioned across ^{36}Ar, ^{38}Ar, and ^{40}Ar using the percent isotope abundances extracted in this study from the descent profile (70 eV) at ≤ 5 km (44.3 ± 0.4% ^{36}Ar, 8.5 ± 0.2% ^{38}Ar, and 47.3 ± 0.4% ^{40}Ar).
- We obtain a $(k_i^a)^E$ for ^{84}Kr ($a \leq 23$ km) by comparing the calculated and averaged mixing ratio for ^{84}Kr from ≤23 km to measures obtained by V11/12 for ^{84}Kr at ≤23 km (0.650 ± 0.150 ppm), as obtained using electron ionization mass spectrometers (EI-MS) and reported in Istomin *et al.*, 1978 [21].
- We obtain a $(k_i^a)^E$ for ^{132}Xe ($a \leq 23$ km) by comparing the summed and calculated mixing ratios for ^{131}Xe and ^{132}Xe from ≤23 km to measures obtained by Venera 13 and 14 (V13/14) for the summed mixing ratios of ^{131}Xe and ^{132}Xe at ≤23 km (0.01–0.1 ppm), as obtained using EI-MS and reported in Istomin *et al.*, 1982 [25]. We assume that the $(k_i^a)^E$ for ^{132}Xe is equal to the $(k_i^a)^E$ obtained from the total sums of ^{131}Xe + ^{132}Xe.

In Fig. 2, we compare trends against mass for the reciprocals of $(k_i^a)^I$, $(k_i^a)^E$, and k_i'. Notably, values for ^{20}Ne and ^{36}Ar from the internal ($(k_i^a)^I$) and external ($(k_i^a)^E$) scales are within error, which validates our comparative approach to correct for instrument biases. When considering the external scale ($(k_i^a)^E$; blue squares), power regression across *m/z* 4–40 ($R^2 = 0.9999$) suggests a potential low-mass bias throughout getter retention, pumping, and/or detection. We obtain similar mass-dependent trends across *m/z* 4–84 when including the V11/12 measurement for ^{84}Kr ($R^2 = 0.9998$). However, values for ^{84}Kr from the external (blue square) and internal (red circle and green diamond) scales differ by ~10–100-fold, which is suggestive of overestimation in the V11/12 measurements *or* underestimation by the LNMS conversion factors. Given this uncertainty, the trend across *m/z* 4–84 is displayed separately in Fig. 2 (dashed blue line). For ^{132}Xe, the external (blue square) scale yields values that are *inconsistent* with the trends across *m/z* 4–40 (or *m/z* 4–84); yet are within error to those from the internal scale (red circle and green diamond), thus supporting a high mass bias for the noble gases in the LNMS. Therefore, when considering the bulk LNMS behavior, these trends are suggestive of both low and high-mass biases where He^+ and Xe^+ (and Kr^+) are associated with higher outputted counts and requirements for greater correction.

We suggest that the potential over-representations of He^+ and Xe^+ (and Kr^+) in the LNMS are due to spectrometer design, which possibly yielded low and high mass ions with higher relative kinetic energies upon detection in the respective low and high mass channels – when compared to Ne^+ and Ar^+. Design influences include the compact magnetic sector (~4500 G[1]) and detector arrangement, where low mass ions (*m/z* ≤ 16) were detected just after entry into the magnetic sector in the low-mass channel, while the higher mass ions (*m/z* 15–208) were detected after complete passage through the magnetic sector in a high-mass channel (block diagram, Fig. 2, [1]).

Mass spectral studies [26,27] show that higher relative counts are associated with multiple charged ions (*e.g.*, Xe^{2+}, Xe^{3+}) due to the higher relative kinetic energies acquired after acceleration through the magnetic sector and across the potential difference between the ion source and detector. Analogously, low mass He^+ ions in the LNMS may have exhibited greater relative increases in velocity upon entry into the magnetic sector, thereby yielding enhanced responses in the low mass channel. For Xe^+ and Kr^+, we posit that the compact LNMS design and voltage ramp[1] (~150–2500 V) promoted higher relative increases in velocity after transmission through the magnetic sector and that the substantially higher masses of the incoming ions – when compared to Ar^+ and Ne^+ – yielded enhanced responses in the high-mass channel.

Using the low-mass trends, we are also able to obtain the correction factor ($(k_i^a)^E$) for methane (CH_4, *m/z* 16) via interpolation using the respective regression equation in Fig. 2 (external scale; blue squares). Methane was an internal calibrant gas in the LNMS that *unexpectedly* and *significantly* increased in abundance throughout the descent [8,11]. After correction using Eq. (12) (assumed standard 1 σ error of 34.1%), we obtain updated [11] mixing ratios for methane of 37 ± 13 ppm and 300 ± 102 ppm at 51.3 and 21.6 km, respectively; alternatively expressed as a range of ~40–3000 ppm across ~60 to 1 km. In comparison, our range is much lower than the original reported value of ~1000–6000 ppm methane (~60 to 1 km), especially for the cloud data [8]. However, our values are well above the approximated upper limits of ~10 and 0.6 ppm at 51.6 and 21.6 km, as suggested by the lack of methane detection by the LGC [20]. Hence, these total trends suggest that more extensive corrections for methane (and potentially He) are required or that methane was formed by spacecraft degradation proximal to the LNMS inlet assembly and distal to the LGC inlet, as

$$(ratio)_i^{CO_2} = \frac{n_i}{n_{CO_2}} = \frac{V_i}{V_{CO_2}} \Longrightarrow \frac{w_i}{w_{CO_2}} = \frac{(kg\ m^{-3})_i}{(kg\ m^{-3})_{CO_2}} \Longrightarrow \frac{(kg\ m^{-3})_i}{(kg\ m^{-3})_{CO_2}} \times (kg\ m^{-3})_{CO_2} = (kg\ m^{-3})_i$$

Scheme 1. Diagram for conversion of counts (n_i) to density.

described in Mogul et al., 2023 [11]. Potential sources of spacecraft degradation include the Kapton wiring insulation used in the pyrotechnic devices that removed the LNMS inlet cover prior to sampling [11,23].

Conversion of counts to density

The procedure to convert volume ratio (or percent) to density for a target species ($(kg\ m^{-3})_i$) is outlined in Scheme 1. We calculate the number density ratio against CO_2 ($(ratio)_i^{CO_2}$), which is alternately expressed as the volume ratio against CO_2 (V_i/V_{CO_2}), using the respectively modified version of Eq. (12) (*e.g.*, exclusion of n_{N_2}). The volume ratio is then converted to weight ratio against CO_2 (w_i/w_{CO_2}). The weight ratio (kg_i/kg_{CO_2}), in turn, is equal to the density ratio against CO_2 due to the equal volumes ($(kg\ m^{-3})_i/(kg\ m^{-3})_{CO_2}$). Hence, density of the target species (at the altitude of measurement) is obtained by multiplication of the respective weight ratio (or percent) by the density of CO_2 (at the altitude of measurement). Enabling this conversion are the CO_2 densities at differing altitudes ($(kg\ m^{-3})_{CO_2}$) obtained in Mogul *et al.*, 2023 [11]. Current propagation of total errors, including error for I_i [11], yields densities with uncertainties of (1) ~18% for fitted targets with m/z 15–50 [11], (2) ~23% for non-fitted targets with m/z 15–50, and (3) ~39% for targets with < m/z 15 and > m/z 50.

Methods discussion

Our treatment of the PV LNMS data yields mixing ratios and volume percent values that are consistent with other spacecraft measures, especially the PV LGC. The LNMS (65°) and LGC (265°) sampled Venus' atmosphere using inlets on opposing sides of the PVLP. Our measures for H_2O and SO_2 are within error to the LGC measurements in the clouds (51.6 km) and lower atmosphere (21.6 km). Similarly, our volume percent value for N_2 at 24.4 km is within error to LGC (21.6 km) and V11/12 (23.0 km) measurements. These combined comparisons, therefore, substantiate the strategy of our analytical treatment of the LNMS data and provide a unified measure of Venus' atmosphere from the PVLP (LNMS and LGC). For the noble gases, which require substantial correction due to getter and detector biases, we treat the LNMS data as relative scales with LGC and Venera measurements serving as calibration points. Future efforts will harness these combined methods, conversions, and calibrations to provide new altitude profiles (~64–1 km) for active and noble gases across Venus' atmosphere.

Ethics statements

This work *did not* involve human subjects, animal experimentation, or data collected from social media platforms.

Declaration of Competing Interest

The authors declare that they have no known competing financial interests or personal relationships that could appear to influence the work reported in this paper.

CRediT authorship contribution statement

R. Mogul: Conceptualization, Methodology, Formal analysis, Writing – original draft. **G. Avice:** Writing – review & editing. **S.S. Limaye:** Writing – review & editing. **M.J. Way:** Writing – review & editing.

Data availability

data is already shared by NASA

Acknowledgments

RM acknowledges administrative support from the Blue MarblA Institute of Science and funding from the National Aeronautics and Space Administration (NASA) Nexus for Exoplanet System Science (NExSS) award 80NSSC21K1176. MJW acknowledges support from the GSFC Sellers Exoplanet Environments Collaboration (SEEC) and ROCKE-3D projects, which are funded by the NASA Planetary Science and Earth Science Divisions Internal Scientist Funding Model. MJW was supported by the NASA Astrobiology Program through collaborations arising from his participation in the NExSS and the NASA Habitable Worlds Program. SSL was supported by NASA (NNX16AC79G). GA acknowledges the French Centre National d'Etudes Spatiales (CNES) for it's funding support for Venus-related studies.

References

[1] J.H. Hoffman, R.R. Hodges, K.D. Duerksen, Pioneer Venus large probe neutral mass spectrometer, J. Vac. Sci. Technol. 16 (1979) 692–694.
[2] J.H. Hoffman, et al., Pioneer Venus sounder probe neutral gas mass spectrometer, IEEE Trans. Geosci. Remote Sens. GE-18 (1980) 80–84.
[3] J.H. Hoffman, R.R. Hodges, M.B. McElroy, T.M. Donahue, M. Kolpin, Composition and structure of the Venus atmosphere: results from Pioneer Venus, Science 205 (1979) 49–52.
[4] J.H. Hoffman, R.R. Hodges, M.B. McElroy, T.M. Donahue, M. Kolpin, Venus lower atmospheric composition: preliminary results from Pioneer Venus, Science 203 (1979) 800–802.
[5] J.H. Hoffman, R.R. Hodges, T.M. Donahue, M.B. McElroy, Composition of the Venus lower atmosphere from the Pioneer Venus mass spectrometer, J. Geophys. Res. Space Phys. 85 (1980) 7882–7890.
[6] T. Donahue, J. Hoffman, R. Hodges Jr., Krypton and xenon in the atmosphere of Venus, Geophys. Res. Letters 8 (1981) 513–516.
[7] T.M. Donahue, R.R. Hodges Jr., Past and present water budget of Venus, J. Geophys. Res. 97 (1992) 6083–6091.
[8] T.M. Donahue, R.R. Hodges, Venus methane and water, Geophys. Res. Lett. 20 (1993) 591–594, doi:10.1029/93GL00513.
[9] T.M. Donahue, J.H. Hoffman, R.R. Hodges, A.J. Watson, Venus was wet - a measurement of the ratio of deuterium to hydrogen, Science 216 (1982) 630–633.
[10] R. Mogul, S.S. Limaye, M. Way, J.A. Cordova, Venus' mass spectra show signs of disequilibria in the middle clouds, Geophys. Res. Letters 48 (2021) e2020GL091327, doi:10.1029/2020GL091327.
[11] R. Mogul, S.S. Limaye, M.J. Way, The CO_2 profile and analytical model for the Pioneer Venus Large Probe neutral mass spectrometer, Icarus 392 (2023) 115374, doi:10.1016/j.icarus.2022.115374.
[12] R.O. Fimmel, L. Colin, E. Burgess, Pioneering Venus: A Planet Unveiled, NASA, 1995.
[13] S.S. Limaye, et al., Venus atmospheric thermal structure and radiative balance, Space Sci. Rev. 214 (2018) 102, doi:10.1007/s11214-018-0525-2.
[14] M.A. Bullock, D.H. Grinspoon, The atmosphere and climate of Venus, Comparat. Climatol. Terrest. Planet. 1 (2013) 19–54.
[15] T. Giorgi, B. Ferrario, B. Storey, An updated review of getters and gettering, J. Vac. Sci. Technol. 3 (1985) 417–423.
[16] S.P. Garg, E.A. Gulbransen, P. Vijendran, Zr powder and Zr-16% Al alloy as getters for O2, H2, H2O, CO and CO2 gases, Vacuum 40 (1990) 275–280.
[17] W.E. Wallace, "Mass Spectra" in NIST Chemistry WebBook, NIST Standard Reference Database Number 69, National Institute of Standards and Technology, Gaithersburg MD, 20899, 2020 Available at.
[18] D. Rapp, P. Englander-Golden, Total cross sections for ionization and attachment in gases by electron impact. I. Positive ionization, J. Chem. Phys. 43 (1965) 1464–1479.
[19] V.I. Oyama, G.C. Carle, F. Woeller, Corrections in the Pioneer Venus sounder probe gas chromatographic analysis of the lower Venus atmosphere, Science 208 (1980) 399–401.
[20] V.I. Oyama, et al., Pioneer Venus gas chromatography of the lower atmosphere of Venus, J. Geophys. Res. 85 (1980) 7891–7902.
[21] Istomin, V., Grechnev, K. & Kochnev, V. Mass spectrometry measurements of the lower atmosphere of Venus. (NASA Technical Reports Server; 1978) Available at: https://ntrs.nasa.gov/citations/19790017794.
[22] N.M. Johnson, M.R. de Oliveira, Venus atmospheric composition *in situ* data: a compilation, Earth Space Sci. 6 (2019) 1299–1318.
[23] A. Seiff, et al., Pioneer Venus 12.5 Km Anomaly Workshop Report (Volume I), 1, NASA, Ames Research Center, 1995.
[24] V.A. Krasnopolsky, G.R. Gladstone, Helium on Mars and Venus: EUVE observations and modeling, Icarus 176 (2005) 395–407.
[25] V. Istomin, K. Grechnev, V. Kochnev, Mass spectrometry on the VENERA-13 and VENERA-14 landers-preliminary results, Sov. Astron. Let. 8 (1982) 211–215.
[26] R. Fox, Multiple ionization in argon and krypton by electron impact, J. Chem. Phys. 33 (1960) 200–205.
[27] B. Schram, A. Boerboom, W. Kleine, J. Kistemaker, Amplification factors of a particle multiplier for multiply charged noble gas ions, Physica 32 (1966) 749–761.